

PAPER

3D cross-bended metasurfaces with polarization insensitivity and high-Q resonances

To cite this article: Ruhao Pan *et al* 2020 *J. Opt.* **22** 105103

View the [article online](#) for updates and enhancements.



IOP | ebooks™

Bringing together innovative digital publishing with leading authors from the global scientific community.

Start exploring the collection—download the first chapter of every title for free.

3D cross-bended metasurfaces with polarization insensitivity and high-Q resonances

Ruhao Pan¹ , Shuo Du^{1,2}, Zhe Liu³, Wei Zhu¹, Ce Li^{1,2}, Changzhi Gu^{1,2,5} and Junjie Li^{1,2,4,5}

¹ Beijing National Laboratory for Condensed Matter Physics, Institute of Physics, Chinese Academy of Sciences, Beijing 100190, People's Republic of China

² School of Physical Sciences, CAS Key Laboratory of Vacuum Physics, University of Chinese Academy of Sciences, Beijing 100049, People's Republic of China

³ Center for Hybrid Quantum Networks (Hy-Q), The Niels Bohr Institute, University of Copenhagen, DK-2100, Copenhagen Ø, Denmark

⁴ Songshan Lake Materials Laboratory, Dongguan, Guangdong 523808, People's Republic of China

E-mail: jjli@iphy.ac.cn

Received 1 July 2020, revised 21 July 2020

Accepted for publication 7 August 2020

Published 8 September 2020



Abstract

Metasurfaces with high-quality (HQ) resonances are always desired for their potential applications in biomedicine and photonic devices. However, the realization of HQ near-infrared metasurfaces with polarization insensitivity has faced problems with metallic loss, large feature size and limited configurations. In order to build up HQ metasurfaces working at the near-infrared range, we propose a 3D bended metasurface configuration consisting of a metallic supported frame and cross vertical split ring resonators, which are fabricated by a focused ion beam defined origami method. The relationship between Q factor/modulation depth of the resonances and the geometric morphology of the meta-atoms are established, and its polarization insensitivity is verified. Two HQ resonances with 22%/26% modulation depth and the quality factor of 24/30 at 1.75/2.5 μm are experimentally obtained in the optimized metasurface. In addition, a polarization insensitive Fano resonance with large modulation depth can also be observed at the low frequency band, which can be modulated by tuning the bending angle. This HQ 3D cross-bended metasurface will create a more flexible approach to design versatile micro/nano-photonic devices and biological components.

Keywords: FIB defined Origami, high quality factor, Fano resonance, 3D bended metasurface

(Some figures may appear in colour only in the online journal)

1. Introduction

Metasurfaces are artificial electromagnetic structures consisting of subwavelength resonators or meta-atoms, which exhibit

exotic properties such as negative permeability and permittivity, extraordinary optical transmission (EOT) and slow light effects, thus giving rise to new capabilities in modulating light in desired ways [1–6]. Among the fascinating features of the metasurfaces, high-quality (HQ) resonators can produce sharp peaks, which play an important role in their applications of ultrasensitive sensors, high performance filters and

⁵ Authors to whom any correspondence should be addressed.

laser spacers [7–11]. In recent decades, significant efforts have been made to design metamaterials with sharp resonances, and explore their potential applications in photonic devices. A series of HQ metasurfaces ranging from the visible to THz region have been built up based on Fano resonance, trapped mode, bound states in the continuum, etc [7, 12–15]. However, conventional 2D plasmonic metasurfaces are facing problems in control ability and metallic loss, which usually leads to a Q factor lower than 10 [16, 17]. Therefore, a completely new approach is needed for the design of HQ metasurfaces.

Previous reports have found that 3D structures possess higher efficiency, much more controllable degrees of freedom and more functions than their 2D counterparts [18–20]. Thus, 3D metasurfaces with various properties, e.g. electromagnetic invisibility and chiral light regulation, have been developed [21, 22], especially HQ resonances in the infrared region. However, due to the processing limits of traditional micro/nanofabrication methods, such as multilayer stack [23], projection lithography [24] and 3D printing [25], the fabrication of 3D structures with small feature size, abundant spatial freedom, rich optional materials and well controlled configurations have become a huge challenge, which leads to the working band of these metamaterials being larger than $3\ \mu\text{m}$, i.e. in the mid-infrared or even longer range. What is more, polarization insensitive metamaterials can be directly excited by natural light, thus simplifying the device structures and improving the working efficiency [21, 26]. However, planar metamaterials are usually sensitive to the polarization of light due to the asymmetric design of resonators, which leads to a more complex components structure compared to the polarization insensitive one. Up to now, there have been few reports of high-Q metamaterials with polarization insensitivity based on localized surface plasmonic resonances (LSPRs) because of the difficulty of the configuration design [15, 27]. Therefore, a type of polarization insensitive HQ metasurface based on Fano resonance operating in the near-infrared region is needed, for its potential applications in the field of bio-sensing and spectrum enhancement devices. Fortunately, thanks to the advantages of the focused ion beam (FIB), such as the abundant spatial control ability, rapid processing capacity of micro/nanoscale precision and the flexible structure design property, FIB defined origami has been developed in recent years, which can fabricate 3D bending and folding structures in micro/nanoscale with high controllable degrees and rich spatial configurations [28–33]. This enables 3D structures more abilities in constructing 3D metasurface, showing versatile photonic properties such as Fano resonances and giant chirality by their exceptional geometries, and opens up a new horizon in the design of the photonic devices [34, 35].

In this work, we have proposed a kind of 3D bended metasurface, consisting of a supported metallic frame and cross vertical split ring resonators (SRRs), which can generate HQ Fano-shape resonances. In addition, the polarization insensitive effect can be obtained on account of the C4 rotational symmetry of the metasurface. Structures with different configurations have also been simulated by the

finite-difference time-domain (FDTD) method, which demonstrate that as the bending angle increases, the Q factor decreases and the corresponding modulation depth increases. According to the simulation, the optimized metasurface depicts a Q factor of 187 and 308 at $1.75\ \mu\text{m}$ and $2.5\ \mu\text{m}$, respectively. Metasurfaces with different bending angles are fabricated by the FIB defined origami method which contains EBL patterning and FIB global irradiating process. A Fourier transform infrared spectrometer (FTIR) has been used to collect the transmission spectra of the 3D metasurfaces. The results agree well with the simulation that resonances with relatively high Q factor can be observed at $1.75\ \mu\text{m}$ and $2.5\ \mu\text{m}$. Besides, an additional Fano resonance with larger modulation depth is observed in the mid-infrared region, which also changes with the bending angle. The development of this metasurface shows a great application potential in biomedical, free-space optical communications and remote sensing devices.

2. Results and discussion

The schematics of the 3D metasurfaces are depicted in figure 1(a), with a periodic array of plasmonic meta-atoms at the top and geometric parameters at the bottom. Each meta-atom is composed of a supported frame and cross vertical SRRs with a period of $P = 2.5\ \mu\text{m}$, and the width for the bending SRRs and the supported frame is $w = 200\ \text{nm}$. Two vertical SRRs that intersect at the center form a 90° crossed vertical SRRs with a radius of $r = 900\ \text{nm}$. The bending angle of the vertical SRRs is θ , which is defined by the central angle of the bended cantilever and can be changed by tuning the length (l) of the cantilever. The whole structures are fabricated on a bilayer film consisting of $60\ \text{nm}$ Au and $20\ \text{nm}$ SiN_x . Samples with $100\ \mu\text{m} \times 100\ \mu\text{m}$ area can be fabricated flexibly by the FIB defined bending method as shown in the scanning electron micrography (SEM) image of figure 1(b). The processing flow starts from the oxygen plasma cleaning of a $100\ \mu\text{m} \times 100\ \mu\text{m}$ SiN_x window (ilabilab) with $20\ \text{nm}$ SiN_x film. After spin-coating resist, the designed patterns are written by electron beam lithography (EBL, Raith 150). Reactive ion etching (RIE, Oxford NGP 80) is used to transfer the patterns to the SiN_x film, and the Au/ SiN_x bilayer film can be obtained by $60\ \text{nm}$ Au deposition through electron beam evaporation. Finally FIB global irradiation is applied to introduce tensile stress into the planar pattern and form a bended metasurface structure. Large area 3D cross-bended metasurfaces with good uniformity are obtained smoothly, and the bending angle can be precisely controlled by the ion energy and ion dose. The inset in figure 1(b) shows the details of the meta-atom, which is well consistent with the simulation model.

FDTD is introduced to simulate the transmission spectra of each component of the metasurface. Figure 2(a) shows the vertical SRRs with a 130° bending angle, the metallic frame and the 3D bended metasurface. The transmission spectra are shown in figure 2(b), where the black curve is the transmission spectrum of the supported frame showing a typical EOT line shape (continuum state), and the red curve describes the

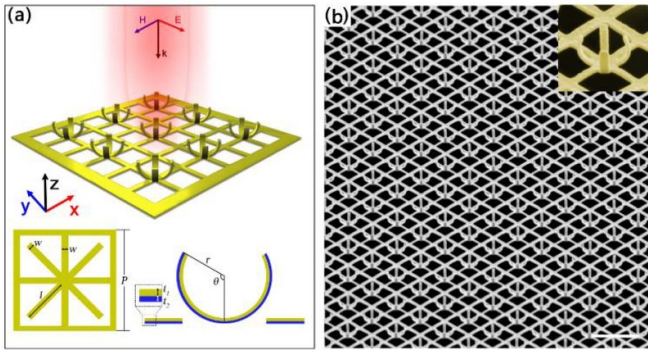


Figure 1. (a) The schematic and the feature sizes of the 3D bended metasurface, where the period of the meta-atoms is $P = 2.5 \mu\text{m}$, and the width and the radius of the cantilevers are $w = 200 \text{ nm}$ and $r = 900 \text{ nm}$. The bending angle (θ) can be tuned by the length (l) of the cantilevers. The whole structure is based on a bilayer film with 60 nm Au and 20 nm SiN_x ; (b) SEM of large scale metasurface fabricated by FIB defined origami, and the inset is a false color image of the bended metasurface. Scale bar: $3 \mu\text{m}$.

property of NIR transmission of the vertical SRRs. Three resonances can be observed from the red curve, in which the resonances at $1.68 \mu\text{m}$ and $2.71 \mu\text{m}$ show sharp dips and asymmetric line shapes due to the interaction of the magnetic and the electric resonance [36, 37]. Although sharp dips are obtained, the modulation depth of the $1.68 \mu\text{m}$ resonance is too shallow to be detected by measurement. Fortunately, the modulation depth becomes deeper after the combination of the vertical SRRs and the frame, as depicted in the blue curve. There are also two HQ resonances appearing in this composite structure. In figure 2(b), it is obvious that the resonance at $1.68 \mu\text{m}$ red-shifts to $1.75 \mu\text{m}$, and the resonance at $2.71 \mu\text{m}$ blue-shifts to $2.5 \mu\text{m}$. Since the Q factor of the Fano resonance is determined by the discrete states, the HQ property of the two resonances is inherited for the two resonances in the red curve mentioned above [38, 39]. Figure 2(c) highlights the polarization insensitivity of the C4 symmetric metasurface, where the spectra of x-polarization and y-polarization incident are totally overlapped, indicating that the 3D bended metasurface is a polarization insensitive one.

The electric field distribution of the resonances at $1.75 \mu\text{m}$ and $2.5 \mu\text{m}$ are also extracted and shown in figures 2(d) and (e), respectively. As shown in the electric field distribution at the height of 100 nm, the electric field of the metallic frame and the vertical SRRs are coupled. Strong near field enhancement can be observed for both resonances, which manifests a strong light confinement effects at corresponding wavelengths. The localized field enhancement effect of the Fano resonance plays an important role in the application of bio-sensing [40, 41]. The coupling of the field also results in a shift of the resonances. Compared to the vertical SRRs without metallic frame, the modulation depth and the Q factor of the composite 3D structure are larger for both resonances. Although the field is relatively weak at the height of 500 nm, the light is highly confined at the surface of the metal, this means that the

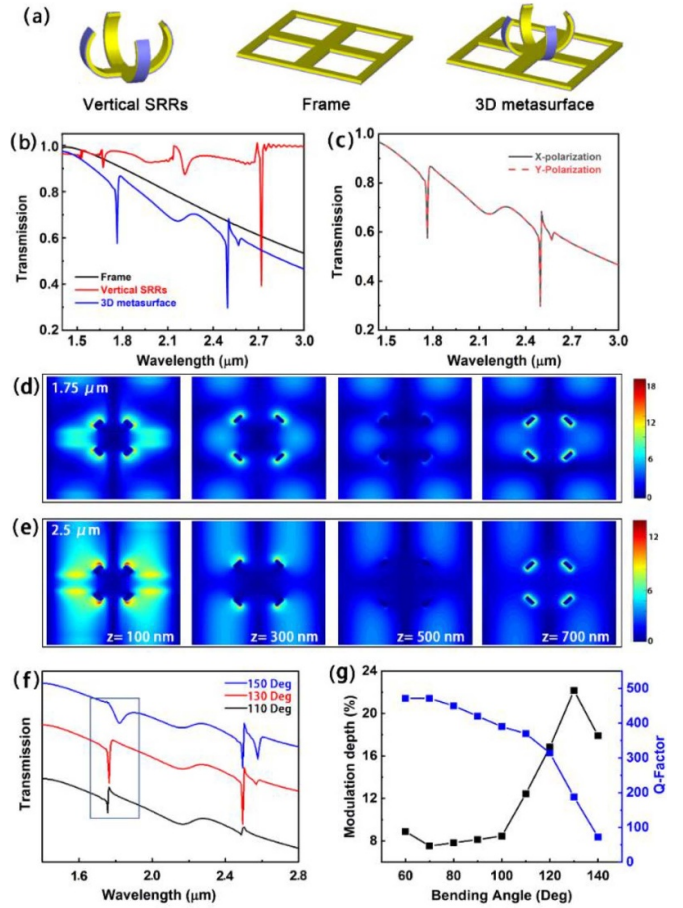


Figure 2. (a) Schematics of the cross vertical SRRs, supported frame and the 3D metasurface, and their transmission spectra are shown in (b), respectively. (c) The spectra of the metasurface for the x-polarization and y-polarization. (d), (e) The electric field distribution of the 3D structures at $1.75 \mu\text{m}$ and $2.5 \mu\text{m}$, respectively. (f) The transmission spectra for metasurfaces with 110° , 130° and 150° bending angles. (g) The Q factor and the modulation depth changes with the bending angle.

light is dissipated by the resonator. The property of the two HQ resonances in one metasurface is conducive to the design of multiplexing devices, and the unexpected perturbation in the spectra at $2.6 \mu\text{m}$ is because of the Wood-Rayleigh anomalies [42, 43].

Quantitative Q factor and modulation depth can be used to determine the properties of the HQ resonance. The Q factor can be calculated by $Q = f_{\text{Center}}/\Delta f$, where f_{Center} and Δf are the center frequency and the full width half maximum of the resonance dip, respectively. The modulation depth is usually defined by the transmission/reflection difference for the modulators with different states [44–46]. However, in this work, the modulation depth of the resonance is the transmission difference of the resonance dip and the edge [9], and the modulation depth indicates the intensity of the resonance. A higher modulation depth is beneficial to the design of high sensitivity bio-sensors and high efficiency optical devices. The

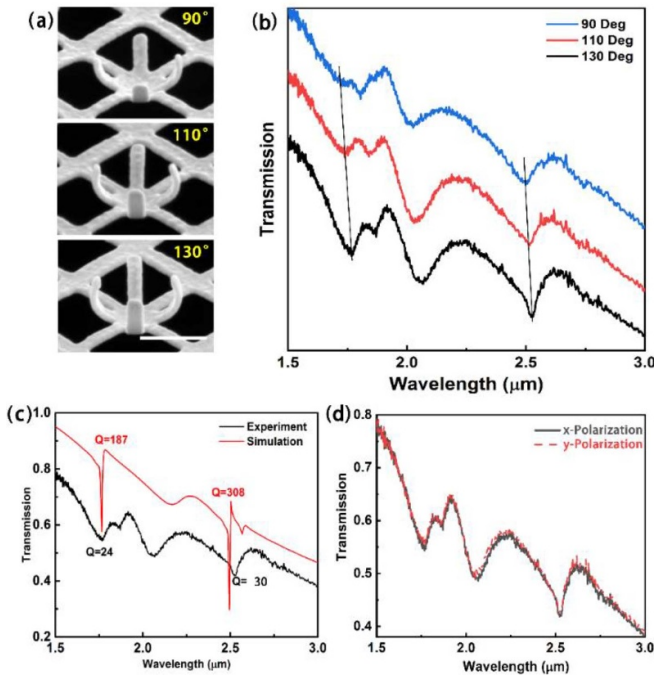


Figure 3. (a) The unit cell of the fabricated metasurfaces. From left to right the bending angles are 90° , 110° and 130° , respectively, and their spectra are shown in (b). (c) A comparison of the simulated and experimental result for 130° bending metasurface. (d) The transmission spectra of the metasurface for x - and y -polarized incident, respectively. Scale bar: (a) $1 \mu\text{m}$.

modulation depth is the transmission difference of the resonance dip and the background curve. For the metasurface with 130° bending angle, the resonance at $1.75 \mu\text{m}$ has a Q factor of 187 with a modulation depth of 22%, and the resonance at $2.5 \mu\text{m}$ has a Q factor of 308 with a modulation depth of 26%.

The metasurfaces with different bending angles are further investigated in order to maximize the Q factors and the modulation depths. Figure 2(f) shows transmission spectra of metasurfaces with 110° , 130° and 150° bending angles, from which it is clear that the modulation depth of the resonance at $2.5 \mu\text{m}$ achieves maximum at 130° bending angle, and dramatically decreases when the bending angle changes. Besides, for the resonance at $1.75 \mu\text{m}$, because the resonance is slowly changed with the geometrical morphology of the structures, the Q factor together with the modulation depth can change with the bending angle. As can be seen from figure 2(g), for the resonance at $1.75 \mu\text{m}$, as the bending angle changes from 60° to 140° , the modulation depth maintains around 8% for the bending angle below 100° , and then sharply increases with the bending angle increasing continuously, and reaches a maximum of 22% at 130° bending angle. Meanwhile, although the Q factor decreases with the increase of the bending angle, a relatively large Q factor of 187 can also be obtained for 130° metasurface. This means the resonances at $1.75 \mu\text{m}$ and $2.5 \mu\text{m}$ attain the highest modulation depth at a premise of HQ factor for the metasurface with 130° bending angle.

According to the schematic in figure 1, by tuning the length of the C4 symmetric cantilevers, metasurfaces with different bending angles can be fabricated by the FIB defined origami method, and large area metasurfaces with excellent uniformity can be obtained. Figure 3(a) gives the SEM images of unit cells with different bending angles of 90° , 110° and 130° , respectively. A FTIR system (Bruker Vertex 80 v) operating in the range of $1.2 - 4.5 \mu\text{m}$ is used to collect the transmission spectra of the metasurfaces. This instrument is equipped with an incoherent NIR optical source. A sample with $100 \times 100 \mu\text{m}^2$ area is displaced under the microscope (Bruker Hyperion) with $15 \times$ objective lens (A597-15). The working distance and the N.A. of the lens are 24 mm and 0.4 respectively, and an aperture is placed between the sample and the objective to ensure the apex angle of the illumination cone less than 5° . The background signal is collected from the air by 128 times scanning, and then the spectrum of the bended metasurfaces is collected after 128 times scanning. The results shown in figure 3(b) demonstrate the transmission spectra of metasurfaces with different bending angles. On the blue curve (90° bending), it is obvious that the resonances at $1.75 \mu\text{m}$ and $2.5 \mu\text{m}$ do not appear. However, both resonances with small modulation depths appear for the 110° bending metasurface (red curve). What is more, the modulation depth of these resonances is further increased for the 130° bending metasurface, and it is experimentally proved to be an optimized structure. A comparison between the simulation and the experiment of the 130° bending metasurface is shown in figure 3(c), where the line shape of the spectrum reveals that the experiment and the simulation agree well. The experimental Q factor of both resonances are 24 and 30, respectively, which are relative HQ factors for metasurfaces. In addition, there is a small dip appearing at $1.9 \mu\text{m}$, which is due to the undulating surface of the metasurface that introduces a dip angle for the incident. The mismatches in the modulation depth and the Q factor between the simulation and the experiment are mainly caused by the metal loss and imperfections in the experiment. Figure 3(d) demonstrates the x - and y -polarized incident transmission spectra of the 130° metasurface, where the spectra yield to the same line shape, verifying that the C4 symmetry metasurfaces are polarization insensitive, which are also in good agreement with the simulation results.

Besides the HQ Fano resonances at the near-infrared band, a resonance with asymmetric line shape can also be observed in the mid-infrared band, and this resonance generates a red shift with the increasing of the bending angle. Figure 4(a) demonstrates the measured results of the low frequency resonance. The resonance with typical Fano line shape is red shifted from $2.5 \mu\text{m}$ to $4.8 \mu\text{m}$ with the bending angle changes from 30° to 130° , and the modulation depth also changes with the bending angle and reaches a maximum at 50° bending angle. The validity is verified by the simulation in figure 4(b). Figure 4(c) gives the details of the simulated and experimental results for the 50° metasurface, and the resonance wavelength (modulation depth) for the experiment and simulation are $2.91 \mu\text{m}$ (63%) and $3.14 \mu\text{m}$ (72%), respectively, indicating that the measurement and the simulation are

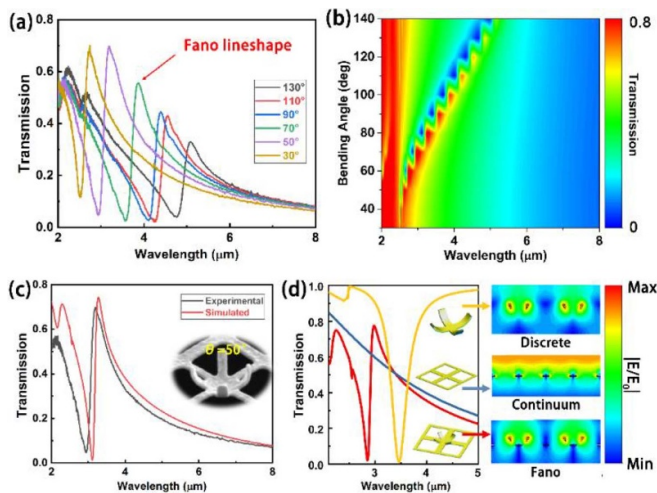


Figure 4. The spectra of the mid-infrared band of the metasurface. (a), (b) The experimental and simulated spectra of the metasurfaces with different bending angles. (c) A comparison between the simulation and the experiment for the metasurface with 50° bending angle. (d) The spectra and the local electric field distribution of the continuum state, discrete state and Fano metasurface.

well consistent. To explore the underlying mechanism of this resonance, the spectra and local electric field distribution at the resonance position of the metallic frame, vertical SRRs, and the Fano metasurface (with bending angle of 50°) are demonstrated in figure 4(d), respectively. From the near-field distribution, it can be found that the Fano resonance is generated by the near-field coupling between the metallic frame (continuum state) and the vertical SRRs (discrete state), and the line shape in the spectrum of Fano metasurface is not a simple superposition of the spectra of the vertical SRRs and the frame, but the coupling between them. The tuning of the bending angle will dramatically affect the intrinsic resonance frequency of the discrete state so that the resonance wavelength and modulation depth of Fano resonance can be modulated.

3. Conclusions

In conclusion, we have brought out a kind of 3D bending metasurface consisting of a metallic frame and cross vertical SRRs in nanoscale, which has two HQ resonances in the near infrared range and shows polarization insensitive property. FDTD simulation reveals that this metasurface can generate HQ resonances at 1.75 μm and 2.5 μm because of the coupling of the EOT spectrum of the supported frame and the electromagnetic mode of the vertical SRRs. The modulation depth and Q factor of the metasurfaces can be modulated by the geometric construction of the vertical SRRs, and HQ resonances with large modulation depth can be obtained by the 130° bending metasurface. The as-designed metasurfaces with different bending angles have been fabricated by FIB defined origami method, and the experimental results confirm perfect polarization insensitive and reveal that the metasurface with 130°

bending angle has Q factors of 24 and 30 at 1.75 μm and 2.5 μm , respectively. Our works not only provide a simple method for design and preparation of HQ 3D metasurface with polarization insensitivity, but also open up a new horizon for their applications of multifunctional photonics devices.

Acknowledgments

The authors acknowledge the financial support received from the National Key Research and Development Program of China (Grant Nos. 2016YFA0200800 and 2016YFA0200400), the National Natural Science Foundation of China (Grant Nos. 11674387, 91323304, and 61905274), China Postdoctoral Science Foundation (Grant No. 2020M670506) and the Key Research Program of Frontier Sciences of Chinese Academy of Sciences (Grant No. QYZDJ-SSW-SLH042).

ORCID iD

Ruhao Pan  <https://orcid.org/0000-0002-5573-2992>

References

- [1] Shaltout A M, Shalaev V M and Brongersma M L 2019 Spatiotemporal light control with active metasurfaces *Science* **364** 648
- [2] Falcone F, Lopetegui T, Laso M A, Baena J D, Bonache J, Beruete M, Marques R, Martin F and Sorolla M 2004 Babinet principle applied to the design of metasurfaces and metamaterials *Phys. Rev. Lett.* **93** 197401
- [3] Yu N and Capasso F 2014 Flat optics with designer metasurfaces *Nat. Mater.* **13** 139–50
- [4] McClung A, Mansouree M and Arbabi A 2020 At-will chromatic dispersion by prescribing light trajectories with cascaded metasurfaces *Light Sci. Appl.* **9** 93
- [5] Zhang X, Li Q, Liu F, Qiu M, Sun S, He Q and Zhou L 2020 Controlling angular dispersions in optical metasurfaces *Light Sci. Appl.* **9** 76
- [6] Dhama R, Caligiuri V, Petti L, Rashed A R, Rippa M, Lento R, Termine R, Caglayan H and De Luca A 2018 Extraordinary effects in quasi-periodic gold nanocavities: enhanced transmission and polarization control of cavity modes *ACS Nano* **12** 504–12
- [7] Fedotov V A, Rose M, Prosvirnin S L, Papasimakis N and Zheludev N I 2007 Sharp trapped-mode resonances in planar metamaterials with a broken structural symmetry *Phys. Rev. Lett.* **99** 147401
- [8] Zhang J, MacDonald K F and Zheludev N I 2014 Giant optical forces in planar dielectric photonic metamaterials *Opt. Lett.* **39** 4883–6
- [9] Yang S, Liu Z, Xia X, Y E, Tang C, Wang Y, Li J, Wang L and Gu C 2016 Excitation of ultrasharp trapped-mode resonances in mirror-symmetric metamaterials *Phys. Rev. B* **93** 235407
- [10] Siddique R H, Kumar S, Narasimhan V, Kwon H and Choo H 2019 Aluminum metasurface with hybrid multipolar plasmons for 1000-fold broadband visible fluorescence enhancement and multiplexed biosensing *ACS Nano* **13** 13775–83
- [11] Wang J, Coillet A, Demichel O, Wang Z, Rego D, Bouhelier A, Grelu P and Cluzel B 2020 Saturable

- plasmonic metasurfaces for laser mode locking *Light Sci. Appl.* **9** 50
- [12] Wang H, Li P, Gao N, Huang K, Kang J, Ji L and Yu E 2018 Asymmetric light reflectance by Fano resonance between Fresnel reflection and localized surface plasmons *Appl. Phys. Express* **11** 092001
- [13] Tian X, Liu Z, Lin H, Jia B, Li Z Y and Li J 2018 Five-fold plasmonic Fano resonances with giant bisignate circular dichroism *Nanoscale* **10** 16630–7
- [14] Wu C, Arju N, Kelp G, Fan J A, Dominguez J, Gonzales E, Tutuc E, Brener I and Shvets G 2014 Spectrally selective chiral silicon metasurfaces based on infrared Fano resonances *Nat. Commun.* **5** 3892
- [15] Liu Z, Xu Y, Lin Y, Xiang J, Feng T, Cao Q, Li J, Lan S and Liu J 2019 High-Q quasibound states in the continuum for nonlinear metasurfaces *Phys. Rev. Lett.* **123** 253901
- [16] Ma M, Li Z, Liu W, Tang C, Li Z, Cheng H, Li J, Chen S and Tian J 2019 Optical information multiplexing with nonlinear coding metasurfaces *Laser Photonics Rev.* **13** 1900045
- [17] Verre R, Shao L, Odebo Lank N, Karpinski P, Yankovich A B, Antosiewicz T J, Olsson E and Kall M 2017 Metasurfaces and colloidal suspensions composed of 3D chiral Si nanoresonators *Adv. Mater.* **29** 1701352
- [18] Valentine J, Zhang S, Zentgraf T, Ulin-Avila E, Genov D A, Bartal G and Zhang X 2008 Three-dimensional optical metamaterial with a negative refractive index *Nature* **455** 376–9
- [19] Leong T G, Zarafshar A M and Gracias D H 2010 Three-dimensional fabrication at small size scales *Small* **6** 792–806
- [20] Ma H F and Cui T J 2010 Three-dimensional broadband and broad-angle transformation-optics lens *Nat. Commun.* **1** 124
- [21] Yang Y, Jing L, Zheng B, Hao R, Yin W, Li E, Soukoulis C M and Chen H 2016 Full-polarization 3D metasurface cloak with preserved amplitude and phase *Adv. Mater.* **28** 6866–71
- [22] Kadic M, Milton G W, van Hecke M and Wegener M 2019 3D metamaterials *Nat. Rev. Phys.* **1** 198–210
- [23] Liu N, Guo H, Fu L, Kaiser S, Schweizer H and Giessen H 2008 Three-dimensional photonic metamaterials at optical frequencies *Nat. Mater.* **7** 31–37
- [24] Burckel D B, Wendt J R, Ten Eyck G A, Ginn J C, Ellis A R, Brener I and Sinclair M B 2010 Micrometer-scale cubic unit cell 3D metamaterial layers *Adv. Mater.* **22** 5053–7
- [25] An B W, Kim K, Lee H, Kim S Y, Shim Y, Lee D Y, Song J Y and Park J U 2015 High-resolution printing of 3D structures using an electrohydrodynamic inkjet with multiple functional inks *Adv. Mater.* **27** 4322–8
- [26] Chen -C-C, Ishikawa A, Tang Y-H, Shiao M-H, Tsai D P and Tanaka T 2015 Uniaxial-isotropic metamaterials by three-dimensional split-ring resonators *Adv. Opt. Mater.* **3** 44–8
- [27] Reed G T, Mashanovich G, Gardes F Y and Thomson D J 2010 Silicon optical modulators *Nat. Photonics* **4** 518–26
- [28] Liu Z, Cui A, Li J and Gu C 2019 Folding 2D structures into 3D configurations at the micro/nanoscale: principles, techniques, and applications *Adv. Mater.* **31** e1802211
- [29] Wu C L, Li F C, Pao C W and Srolovitz D J 2017 Folding Sheets with Ion Beams *Nano Lett.* **17** 249–54
- [30] Supekar O D, Brown J J, Eigenfeld N T, Gertsch J C and Bright V M 2016 Atomic layer deposition ultrathin film origami using focused ion beams *Nanotechnology* **27** 49LT02
- [31] Dai C and Cho J H 2016 In situ monitored self-assembly of three-dimensional polyhedral nanostructures *Nano Lett.* **16** 3655–60
- [32] Liu Z, Du H, Li J, Lu L, Li Z-Y and Fang N X 2018 Nano-kirigami with giant optical chirality *Sci. Adv.* **4** eaat4436
- [33] Pan R, Li Z, Liu Z, Zhu W, Zhu L, Li Y, Chen S, Gu C and Li J 2019 Rapid bending origami in micro/nanoscale toward a versatile 3D metasurface *Laser Photonics Rev.* **14** 1900179
- [34] Li J and Liu Z 2018 Focused-ion-beam-based nano-kirigami: from art to photonics *Nanophotonics* **7** 1637–50
- [35] Chen S, Chen J, Zhang X, Li Z Y and Li J 2020 Kirigami/origami: unfolding the new regime of advanced 3D microfabrication/nanofabrication with folding *Light Sci. Appl.* **9** 75
- [36] Cui A *et al* 2015 Directly patterned substrate-free plasmonic nanograting structures with unusual Fano resonances *Light Sci. Appl.* **4** e308
- [37] Kuznetsov A I, Miroshnichenko A E, Fu Y H, Viswanathan V, Rahmani M, Valuckas V, Pan Z Y, Kivshar Y, Pickard D S and Luk'yanchuk B 2014 Split-ball resonator as a three-dimensional analogue of planar split-rings *Nat. Commun.* **5** 3104
- [38] Liu Z, Li J, Liu Z, Li W, Li J, Gu C and Li Z Y 2017 Fano resonance Rabi splitting of surface plasmons *Sci. Rep.* **7** 8010
- [39] Liu Z, Liu Z, Li J, Li W, Li J, Gu C and Li Z Y 2016 3D conductive coupling for efficient generation of prominent Fano resonances in metamaterials *Sci. Rep.* **6** 27817
- [40] Dabidian N, Kholmanov I, Khanikaev A B, Tatar K, Trendafilov S, Mousavi S H, Magnuson C, Ruoff R S and Shvets G 2015 Electrical switching of infrared light using graphene integration with plasmonic fano resonant metasurfaces *ACS Photonics* **2** 216–27
- [41] Wu C, Khanikaev A B, Adato R, Arju N, Yanik A A, Altug H and Shvets G 2012 Fano-resonant asymmetric metamaterials for ultrasensitive spectroscopy and identification of molecular monolayers *Nat. Mater.* **11** 69–75
- [42] Maradudin A A, Simonsen I, Polanco J and Fitzgerald R M 2016 Rayleigh and Wood anomalies in the diffraction of light from a perfectly conducting reflection grating *J. Opt.* **18** 024004
- [43] Kravets V G, Schedin F and Grigorenko A N 2008 Extremely narrow plasmon resonances based on diffraction coupling of localized plasmons in arrays of metallic nanoparticles *Phys. Rev. Lett.* **101** 087403
- [44] Grinblat G, Abdelwahab I, Nielsen M P, Dichtl P, Leng K, Oulton R F, Loh K P and Maier S A 2019 Ultrafast all-optical modulation in 2D hybrid perovskites *ACS Nano* **13** 9504–10
- [45] Kutttruff J, Garoli D, Allerbeck J, Krahn R, De Luca A, Brista D, Caligiuri V and Maccaferri N 2020 Ultrafast all-optical switching enabled by epsilon-near-zero-tailored absorption in metal-insulator nanocavities *Commun. Phys.* **3** 114
- [46] Wu Z and Xu Y 2018 Design of a graphene-based dual-slot hybrid plasmonic electro-absorption modulator with high-modulation efficiency and broad optical bandwidth for on-chip communication *Appl. Opt.* **57** 3260–7